Journal of Power Sources 257 (2014) 84–89

Contents lists available at ScienceDirect

Journal of Power Sources

journal homepage: www.elsevier.com/locate/jpowsour

Short communication

A dye-sensitized solar cell based on platinum nanotube counter electrode with efficiency of 9.05%

Jihuai Wu*, Ziying Tang, Yunfang Huang, Miaoliang Huang, Haijun Yu, Jianming Lin

Engineering Research Centre of Environment-Friendly Functional Materials, Ministry of Education, Institute of Materials Physical Chemistry, Huaqiao University, Quanzhou, Fujian 362021, PR China

HIGHLIGHTS

- Pt nanotubes (PNTs) are grown on FTO substrates by polycarbonate template method.
- The PNTs show 1D structure, lower resistance, and good electrochemical activity.
- The dye-sensitized solar cell with PNTs electrode achieves an efficiency of 9.05%.
- The efficiency is increased by 25.5% compared to the DSSC with usual Pt electrode.

ARTICLE INFO

Article history:
Received 14 December 2013
Received in revised form
9 January 2014
Accepted 20 January 2014
Available online 28 January 2014

Keywords:
Dye-sensitized solar cell
Platinum nanotubes
Polycarbonate template method
Counter electrode

ABSTRACT

Platinum nanotubes (PNTs) are directly grown on fluorine-doped tin oxide substrates by a facile polycarbonate template method. Morphology observation and electrochemical measurements indicate that the PNTs show a one-dimensional structure, lower charge-transfer resistance, larger exchange current density and higher electrocatalytic activity for iodide/triiodide redox reaction. Using the PNT as counter electrode and MgO as block layer on TiO_2 film, the fabricated dye-sensitized solar cell achieves a light-to-electric energy conversion efficiency of 9.05% under a simulated solar light irradiation of 100 mW cm^{-2}, the efficiency is increased by 25.5% compared to that of DSSC based on conventional Pt counter electrode. Higher efficiency for the PNT electrode is due its one-dimensional nanostructure, large surface area and good electrochemical activity to iodide/triiodide couple.

1. Introduction

Considerable efforts have been devoted to dye-sensitized solar cell (DSSC) since its first prototype was reported in 1991 [1]. While great progress on the DSSC has occurred over the past decades [2–4]. However, how to enhance its efficiency is still a crucial problem. As a component of DSSC, counter electrode plays an important role in the performance of DSSC.

A counter electrode with high conductivity and catalytic activity is indispensable to a high-efficient DSSC. Various conductive materials, such as platinum, graphite, activated carbon, carbon black, graphene single-wall carbon nanotubes, polypyrrole, polyaniline, metal titanium and aluminum are used as the counter electrodes [3,5–8]. However, the performances of these materials are usually lower in comparison with Pt because of its high catalytic activity and corrosion resistance to iodine in electrolyte. And the most Pt counter electrodes are constructed with Pt particle mesoporous film. Different methods, such as thermal decomposition [3], electrodeposition [9], chemical reduction [10] or sputtering [11] have been employed to prepare Pt particles. But, little significant research on the Pt with one-dimensional nanostructure by template method was attempted. On the other hand, the Pt nanostructures show excellent electrocatalytic activity for CO oxidation [12], ethanol oxidation [13] and hydrogen peroxide response [14], it is expected that these properties can be applied in DSSC.

Herein, Pt nanotubes (PNTs) are directly grown on fluorine-doped tin oxide (FTO) glass substrate by a facile polycarbonate (PC) template method. The resultant PNTs show a one-dimensional (1D) nanostructure, high surface-area and good catalytic activity.

2. Experimental

2.1. Materials

Titanium isopropoxide and 4-*tert*-butylpyridine (TBP) were purchased from Fluka and used as received. The organometallic

* Corresponding author.
E-mail address: jhwu@hqu.edu.cn (J. Wu).

0378-7753/$ – see front matter © 2014 Elsevier B.V. All rights reserved.
http://dx.doi.org/10.1016/j.jpowsour.2014.01.090

compound sensitized dye N-719 [$RuL_2(NCS)_2$, L = 4,4′-dicarboxylate-2,2′-bipyridine] was obtained from Solaronix SA (Switzerland). Chemical reagents including iodine, lithium iodide, tetramethyl ammonium iodine, isopropanol, chloroplatinic acid (H_2PtCl_6), OP emulsification agent (Triton X-100) and other reagents were obtained from Shanghai Chemical Agent, P.R. China and used as received. Conductive glass substrates (fluorine doped tin oxide overlayer, FTO glass) were purchased from Hartford Glass, U.S., and were used as substrates for precipitating porous TiO_2 films and Pt counter electrodes.

2.2. Synthesis of Pt nanotubes (PNTs)

Fig. 1 shows the preparation process of Pt nanotubes. Polycarbonate (PC) template was immersed in 0.5 wt.% H_2PtCl_6 isopropanol solution. After the fully adsorption of H_2PtCl_6 solution for 12 h, the template was transferred and clipped onto FTO glass substrate. Then the substrate was heated at 115 °C for 12 h, which caused the volatilization of isopropanol and the thermal decomposition of H_2PtCl_6, thus, the Pt particles uniformly grown along the PC wall. Finally, the PC template was removed by thermal decomposing at 450 °C for 30 min. For comparison, conventional Pt particles (CPPs) were prepared by conventional thermal decomposition method according to reference [15].

2.3. Preparation of TiO_2 electrodes and fabrication of DSSCs

A TiO_2 colloid was prepared according to the method previously reported [16–18]. Cleaned FTO glass substrates were first treated with 150 mM of $TiCl_4$ isopropanol solution at 70 °C for 12 h. A TiO_2 double layer film with a 10-μm-thick and particles size of 10–20 nm layer, and a 4-μm-thick and particles size of 100–150 nm layer [16] was prepared by coating the TiO_2 colloid on the $TiCl_4$-treated FTO substrate using a doctor blade technique. The area of effective photoanode is 1 × 1 cm^2. Additionally, a small amount of $Mg(CH_3COO)_2$ was added into TiO_2 colloid to form block layer [19]. DSSC was assembled by the methods as described previously [16–18].

2.4. Characterization and measurements

Scanning Electronic Microscope (SEM) images were recorded with an S-4800 instrument (Japan) at an acceleration voltage of 5 kV. The cyclic voltammograms (CVs) of samples was measured in a three-electrode electrochemical cell with an electrochemical workstation (model: CHI 660C, Shanghai Chenhua Co., Ltd) by using Pt electrode as working electrode, a Pt-foiled as counter electrode and a saturated Ag/AgCl as reference electrode dipped in an acetonitrile solution of 100 mM $LiClO_4$, 10 mM LiI and 1 mM I_2, at a scan rate of 50 mV s^{-1}. Electrochemical impedance spectroscopy (EIS) was performed using a sandwich cell configuration with symmetric electrodes in an acetonitrile electrolyte containing 0.05 M I_2, 0.1 M LiI, 0.6 M tetrabutyl ammonium iodide and 0.5 M TBP. A 50 μm Surlyn film was used to separate the films and to seal the cells [20,21]. Tafel polarization measurements were carried out by similar method as the EIS tests.

The photovoltaic test of DSSC was carried out by measuring the current–voltage (J–V) characteristic curves under simulated solar illumination with intensity of 100 mW cm^{-2} (AM 1.5) from a 100 W xenon arc lamp (XQ-500W, Shanghai Photoelectricity Device Company, China) in ambient atmosphere. The fill factor (FF) and light-to-electric energy conversion efficiency (η) of the cell were calculated according to the following equations [3]:

$$FF = \frac{V_{max} \times J_{max}}{V_{oc} \times J_{sc}} \quad (1)$$

$$\eta(\%) = \frac{V_{max} \times J_{max}}{P_{in}} \times 100\% = \frac{V_{oc} \times J_{sc}}{P_{in}} \times 100\% \quad (2)$$

Where J_{SC} is the short-circuit current density (mA cm^{-2}), V_{OC} is the open-circuit voltage (V), P_{in} is the incident light power, and J_{max} (mA cm^{-2}) and V_{max} (V) are the current density and voltage in the J–V curves at the point of maximum power output, respectively.

3. Results and discussion

3.1. Morphology analysis

Fig. 2 (a) shows the SEM image of PC template, the template has an even hole distribution, which provides enough nanochannels for the growth of PNTs. The choice of PC template is due to its flexibility and easy adhering to the conductive glass. Fig. 2 (b) shows the SEM image of resultant Pt nanotubes (PNTs) on FTO glass, it can be seen that deposited platinum shows a hollow tube morphology, the nanotube length and diameter is depends on the hole properties of the PC template. From the magnified SEM image shown in Fig. 2 (c), many Pt nanoparticles exist on the outside of the nanotubes, which enhances the PNT surface roughness and area. For comparison, conventional Pt particles (CPPs) were prepared [9] and shown in Fig. 2 (d), the CPP film has a compact surface and a lower surface-area. Owing to its 1D nanostructure and high surface-area, PNT electrode is expected to have a much improved electrochemical performance.

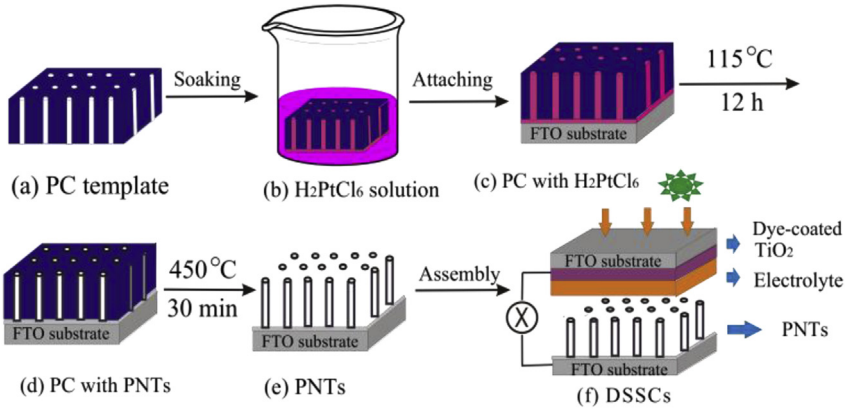

Fig. 1. Preparation process of Pt nanotubes.

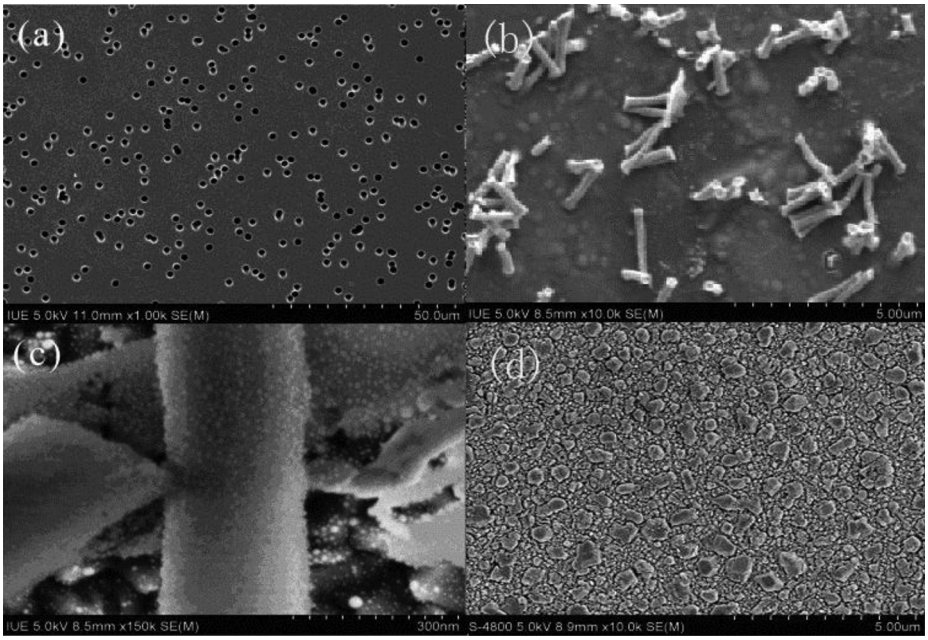

Fig. 2. (a) SEM image of PC template, (b) SEM image of PNTs, (c) magnified SEM image of PNTs, (d) SEM image of conventional Pt nanoparticles.

3.2. Electrochemical analysis

Fig. 3 (a) shows the cyclic voltammogram (CV) for PNT and CPP electrodes at a scan rate of 50 mV s^{-1}, in which two pairs of redox peaks can be observed for both of the electrodes. The cathodic peak (negative current) is assigned to the reduction of I_3^- (Eq. (3)) and the anodic peak (positive current) is assigned to the reverse reaction (Eq. (4)) [6].

$$3I^- - 2e \rightarrow I_3^- \quad (3)$$

$$I_3^- + 2e \rightarrow 3I^- \quad (4)$$

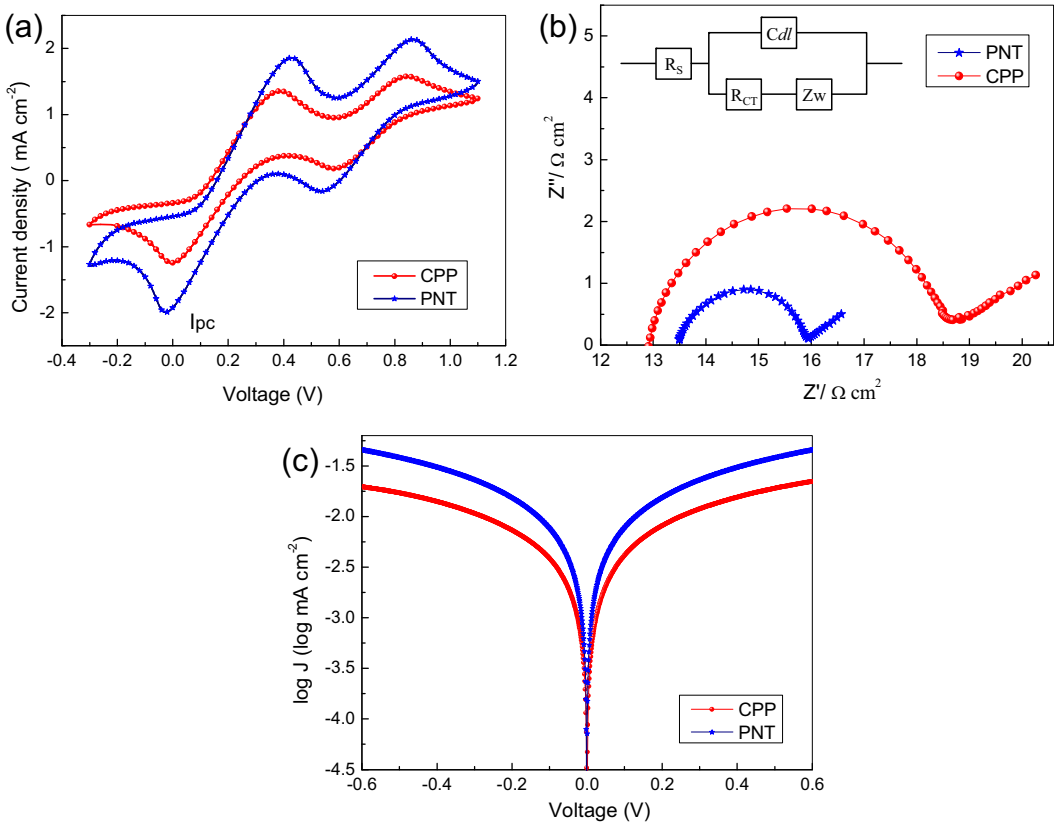

Fig. 3. (a) CV for PNT and CPP electrodes, scan rate = 50 mV s^{-1}. (b) EIS spectra of the symmetrical dummy cells fabricated with two identical PNT and CPP electrodes, frequency range from 100 kHz to 0.1 Hz; (c) Tafel curves of the symmetrical dummy cells fabricated with two identical PNT and CPP electrodes.

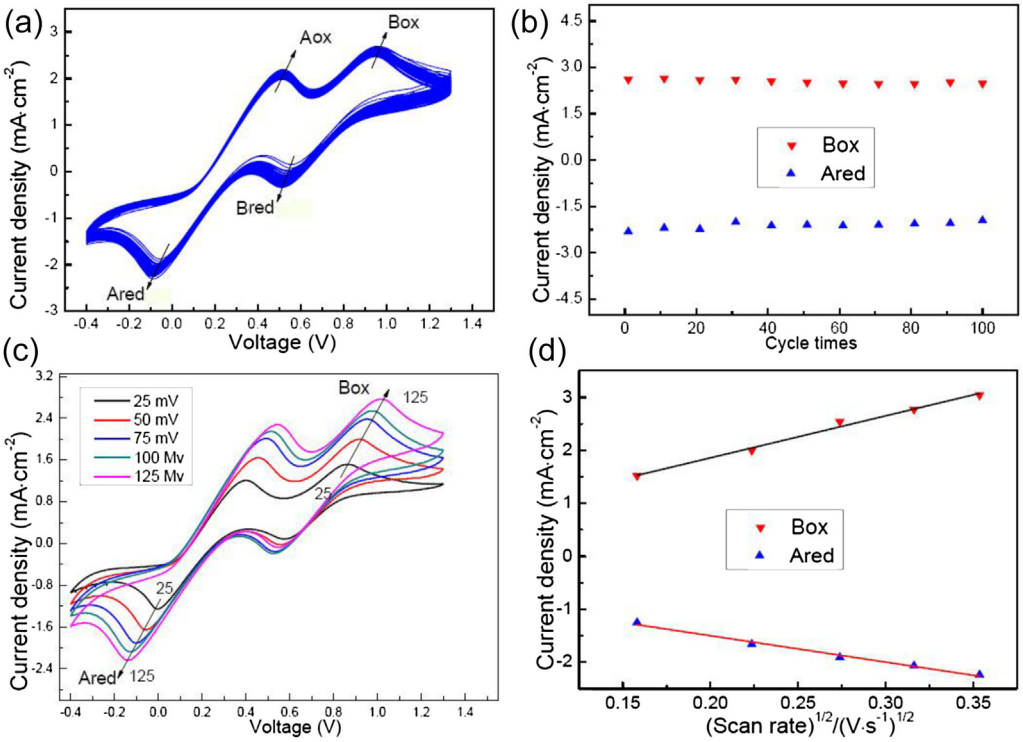

Fig. 4. (a) CVs of PNT electrode for cycle time = 100, scan rate = 100 mV s^{-1}; (b) The relationship between the cycle times and the maximum oxidation and reduction peak currents for PNT electrodes, scan rate = 100 mV s^{-1}; (c) CVs for PNT electrode with different scan rates (from inner to outer: 25, 50, 75, 100, 125 mV s^{-1}); (d) The oxidation and reduction peak currents versus square root of scan rates.

The PNT electrode has a larger current density for the I_3^- reduction and I^- oxidation than that of CPP electrode. The cathodic peak current (Ipc) on the PNT electrode is −1.978 mA cm^{-2}, and which is 1.6 times of that on the CPP electrode (−1.237 mA cm^{-2}), which means a faster redox reaction rate and a better electrocatalytic activity for I_3^-/I^- redox couple on the PNT electrode.

The EIS spectra for the symmetrical cells fabricated with two identical PNT and CPP electrodes are shown in Fig. 3 (b). The charge-transfer resistance (R_{ct}) of PNT electrode is 1.22 Ω cm^2 and which is smaller than that of CPP electrode (2.91 Ω cm^2), the smaller R_{ct} benefits the I_3^-/I^- redox reaction, which is consistent with the CV results in Fig. 3 (a). Similar phenomena were also reported in TiO_2 nanotubes [22] and carbon nanotubes [23] in DSSCs. Detailed studies indicated [24,25] that the charge recombination in nanotubes is much slower than that in nanoparticles, and which results in an improved charge collection efficiency. Since the transporting resistant of charge carriers passing through 1D nanostructures is smaller than that crossing random particles, in the latter case, more interfaces and interspaces between nanoparticles baffle the transportation of charge carriers, or the charge carriers are captured in the interfaces and interspaces.

To further investigate the interfacial charge-transfer properties of the I^-/I_3^- redox couple on the electrode surface, Tafel polarization characterizations were carried out in a dummy cell similar to the one used in the EIS measurements [26,27]. Fig. 3 (c) shows the Tafel curves of the dummy cells based on PNT and CPP electrodes, the curves show logarithmic current density (log J) as a function of voltage (V). In the Tafel zone, the anodic and cathodic branches of PNT electrode shows a larger slope in comparison with that of CPP electrode, which indicates the presence of a larger exchange current density (J_0) on the PNT electrode surface. This means that the PNT electrode has superior catalytic activity for I_3^- reduction. In

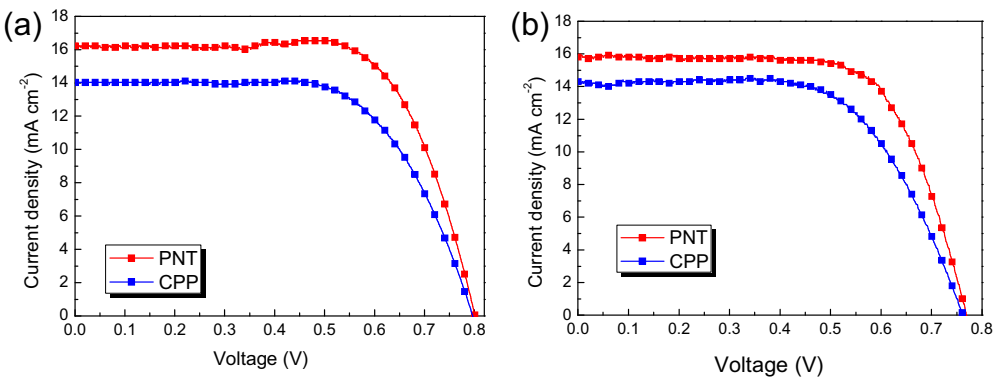

Fig. 5. Photocurrent–voltage curves of the DSSCs based on PNT and CPP electrodes (a) with and (b) without MgO layer on TiO_2 films.

Table 1
Photovoltaic parameters of DSSCs.[a]

DSSC character	J_{SC} (mA cm^{-2})	V_{OC} (V)	FF	η (%)
PNT electrode and MgO layer	16.0	0.801	0.698	9.05
CPP electrode and MgO layer	14.0	0.797	0.645	7.21
PNT electrode without MgO layer	15.8	0.769	0.692	8.41
CPP electrode without MgO layer	14.3	0.763	0.631	6.87

[a] Irradiation source: AM 1.5 G solar simulator (100 mW cm^{-2}) at room temperature.

theory, J_0 varies inversely with R_{ct} as shown in (Eq. (5)) [26]. Combined with the EIS results, the PNT electrode shows a lower R_{ct}, which is well agreement with Tafel polarization measurements on the whole.

$$J_0 = \frac{RT}{nFR_{ct}} \tag{5}$$

Where R is the gas constant, T is the temperature, F is the Faraday constant, and n is the number of electrons exchanged in the reaction at the electrolyte and counter electrode interface.

Briefly, the CV, EIS measurement and Tafel polarization results indicate that the PNT electrode behaves a superior catalytic activity for I_3^- reduction, it can be logically expected that a DSSC based on PNT electrode will achieve an improved photovoltaic performance.

In order to investigate the stability of PNT electrode, the CVs of the electrode were measured. Fig. 4(a) and (b) show 100 consecutive CV cycles of the PNT electrodes at a scan rate of 100 mV s^{-1}. During 100 successive CV cycles, no observable peak current change is found, suggesting that the PNT is stably immobilized on the electrode. On 100 successive scans, though the peak current density changes with the scan voltage, the oxidation and reduction peak current scarcely show change, indicating that the PNT electrode is uniform and stably immobilized on the FTO glass and has an excellent electrochemical stability [28,29].

Fig. 4(c) and (b) illustrate a relationship between the peak current density and the square root of the scan rate, the current density versus $v^{1/2}$ plots is almost linear. The good linear relationship indicates the diffusion limitation of the I_3^-/I^- redox reaction on Pt electrode, which may be due to the transportation of iodide ions in PNT electrode [28,30,31]. This phenomenon shows that the adsorption of iodide ions is hardly affected by the redox reaction on the PNT electrode surface, and suggests that there is no specific interaction between I_3^-/I^- redox couple and PNT electrode [32].

3.3. Photovoltaic performance of DSSCs

The photocurrent–voltage curves of the DSSCs based on PNT and CPP electrodes (a) with and (b) without MgO layer on the TiO_2 films are shown in Fig. 5 and Table 1. It can be seen that the DSSC based on PNT electrode has a higher short circuit current density (J_{SC}) and higher light-to-electric conversion efficiency (η) than the DSSC based on CPP electrode. According to Fig. 3(a) (b) (c), the PNT electrode has a better electrocatalytic activity, larger exchange current density (J_0) and smaller charge-transfer resistance (R_{ct}) than the CPP electrode, which endows higher I_3^-/I^- redox reaction efficiency on PNT electrode than on CPP electrode. From Fig. 2, the PNT has a rough and accessible surface, which increases the effective electrolyte/electrode contact area [12], thus, more Pt can be utilized to catalyze I_3^- reduction. Additionally, the oriented one-dimensional structures of PNTs provide a free channel for electron transport from the electrode to the electrolyte [25], which enhances the charge collection efficiency by suppressing the charge recombination [22,24]. The above factors result in an improved photovoltaic performance.

Compared with Fig. 5 (a) and (b) (Table 1), MgO block layer on TiO_2 film can improve the efficiency of the DSSCs. The efficiency for the DSSCs with MgO layer is increased by 5.39–7.61% compared to the DSSCs without MgO layer. It is believed [14] that the introduction of MgO layer inactivates the TiO_2 surface and suppresses the dark reaction between TiO_2 surface and I_3^- in the electrolyte. On the other hand, as a Lewis acid, MgO can bond with the carboxyl group on dye and improve dye adsorption, which enhances the performance of the DSSC.

4. Conclusion

In summary, platinum nanotubes (PNTs) are directly grown on FTO substrates by a simple polycarbonate template method. The SEM observation shows a one-dimensional structure for the PNTs. The EIS measurements indicate that the PNT electrode has a lower R_{ct}, larger J_0 and higher electrocatalytic activity for I^-/I_3^- redox reaction. Using the PNTs as counter electrode and MgO as block layer on TiO_2 film, the assembled dye-sensitized solar cell achieves a power conversion efficiency of 9.05% under a simulated solar light irradiation of 100 mW cm^{-2}, the efficiency is increased by 25.5% compared to that of DSSC based on conventional Pt counter electrode. Higher efficiency for the PNT electrode is due its one-dimensional nanostructure, large surface area and good catalytic activity to I_3^-/I^- couple.

Acknowledgments

The authors acknowledge the financial joint support by the National Natural Science Foundation of China (Nos. 90922028, U1205112, 50842027, 61306077) and the specialized research fund for the doctoral program of Higher University, Ministry of Education, China (No. 20123501110001).

References

[1] B. O'Regan, M. Gratzel, Nature 353 (1991) 737.
[2] M. Grätzel, Nature 414 (2001) 338.
[3] A. Hagfeldt, G. Boschloo, L. Sun, L. Kloo, H. Pettersson, Chem. Rev. 110 (2010) 6595.
[4] A. Yella, H. Lee, H. Tsao, C. Yi, A. Chandiran, M. Nazeeruddin, E. Diau, C. Yeh, S. Zakeeruddin, M. Gratzel, Science 334 (2011) 629.
[5] Y. Hu, H. Wang, B. Hu, ChemSusChem 3 (2010) 782.
[6] Q. Meng, H. Sun, Y. Luo, Y. Zhang, D. Li, Z. Yu, K. Li, J. Phys. Chem. C. 114 (2010) 11673.
[7] S. Ahmad, J. Yum, X. Zhang, M. Gratzel, H. Butt, M. Nazeeruddin, J. Mater. Chem. 20 (2010) 1654.
[8] J. Trancik, S. Barton, J. Hone, Nano Lett. 8 (2008) 982.
[9] C. Yoon, R. Lee, W. Chae, K. Kim, Electrochim. Acta 53 (2008) 2890.
[10] G. Khelashvili, S. Behrens, C. Weidenthaler, C. Vetter, A. Hinsch, R. Kern, K. Skupien, E. Dinjus, H. Bonnemann, Thin Solid Films 511 (2006) 342.
[11] V. Dao, S. Kim, H. Choi, J. Kim, H. Park, J. Lee, J. Phys. Chem. C. 115 (2011) 25529.
[12] L. Liu, S.H. Yoo, S. Park, Chem. Mater. 22 (2010) 2681.
[13] X. Zhang, W. Lu, J. Da, H. Wang, D. Zhao, P. Webley, Chem. Comm. 195 (2009).
[14] M. Yang, F. Qu, Y. Lu, Y. He, G. Shen, R. Yu, Biomaterials 27 (2006) 5944.
[15] H. Koo, Y. Kim, Y. Lee, W. Lee, K. Kim, N. Park, Adv. Mater. 20 (2008) 195.
[16] J. Wu, S. Hao, Z. Lan, J. Lin, M. Huang, Y. Huang, P. Li, S. Yin, T. Sato, J. Am. Chem. Soc. 130 (2008) 11568.
[17] Z. Lan, J. Wu, S. Hao, J. Lin, M. Huang, Y. Huang, Energ. Environ. Sci. 2 (2009) 524.
[18] J. Wu, Z. Lan, J. Lin, M. Huang, S. Hao, T. Sato, S. Yin, Adv. Mater. 19 (2007) 4006.
[19] G. Kumara, S. Kaneko, A. Konno, M. Okuya, K. Murakami, Prog. Photovol. 14 (2006) 643.
[20] J. Wu, Y. Xiao, Q. Tang, G. Yue, J. Lin, M. Huang, Y. Huang, L. Fan, Z. Lan, S. Yin, T. Sato, Adv. Mater. 24 (2012) 1884.
[21] J. Roy-Mayhew, D. Bozym, C. Punckt, I. Aksay, ACS Nano 4 (2010) 6203.
[22] J. Jennings, A. Ghicov, L. Peter, P. Schmuki, A. Walker, J. Am. Chem. Soc. 130 (2008) 13364.
[23] P. Dong, C. Pint, M. Hainey, F. Mirri, Y. Zhan, J. Zhang, M. Pasquali, R. Hauge, R. Verduzco, M. Jiang, H. Lin, J. Lou, ACS Appl. Mater. Interfaces 3 (2011) 3157.
[24] K. Zhu, N. Neale, A. Miedaner, A. Frank, Nano Lett. 7 (2007) 69.
[25] Z. Liu, V. Subramania, M. Misra, J. Phys. Chem. C. 113 (2009) 14028.

[26] M. Wu, X. Lin, Y. Wang, L. Wang, W. Guo, D. Qi, X. Peng, A. Hagfeldt, M. Gratzel, T. Ma, J. Am. Chem. Soc. 134 (2012) 3419.
[27] M. Wu, X. Lin, A. Hagfeldt, T. Ma, Angew. Chem. Int. Ed. 50 (2011) 3520.
[28] Q. Li, J. Wu, Q. Tang, Z. Lan, P. Li, J. Lin, L. Fan, Electrochem. Commun. 10 (2008) 1299.
[29] Z. Tang, J. Wu, M. Zheng, J. Huo, Z. Lan, Nano Energy 2 (2013) 622.
[30] Y. Saito, W. Kubo, T. Kitamura, Y. Wada, S. Yanagida, J. Photochem. Photobiol. A 164 (2004) 153.
[31] S. Biallozor, A. Kupniewska, Electrochem. Commun. 2 (2000) 480.
[32] A. Hauch, A. Georg, Electrochim. Acta 46 (2001) 3457.